Journal of
Synchrotron
Radiation

ISSN 0909-0495

Received 14 October 2009
Accepted 30 January 2010

The pathogenesis of Randall's plaque: a papilla cartography of Ca compounds through an *ex vivo* investigation based on XANES spectroscopy

Xavier Carpentier,[a,b] Dominique Bazin,[a]* Paul Jungers,[c] Solenn Reguer,[d] Dominique Thiaudière[d] and Michel Daudon[e]

[a]Laboratoire de Physique des Solides, Bâtiment 510, Université Paris Sud, 91405 Orsay, France, [b]CHU Nice, Hôpital Pasteur, 30 Avenue de la voie romaine, 60000 Nice, France, [c]AP-HP, Hôpital Necker, Service de Néphrologie, 149 Rue de Sèvres, 75743 Paris Cedex 15, France, [d]Synchrotron SOLEIL, L'Orme des Merisiers, Saint-Aubin, BP 48, 91192 Gif-sur-Yvette Cedex, France, and [e]AP-HP, Hôpital Necker, Service de Biochimie A, 149 Rue de Sèvres, 75743 Paris Cedex 15, France. E-mail: bazin@lps.u-psud.fr

At the surface of attached kidney stones, a particular deposit termed Randall's plaque (RP) serves as a nucleus. This structural particularity as well as other major public health problems such as diabetes type-2 may explain the dramatic increase in urolithiasis now affecting up to 20% of the population in the industrialized countries. Regarding the chemical composition, even if other phosphate phases such as whitlockite or brushite can be found as minor components (less than 5%), calcium phosphate apatite as well as amorphous carbonated calcium phosphate (ACCP) are the major components of most RPs. Through X-ray absorption spectroscopy performed at the Ca *K*-absorption edge, a technique specific to synchrotron radiation, the presence and crystallinity of the Ca phosphate phases present in RP were determined *ex vivo*. The sensitivity of the technique was used as well as the fact that the measurements can be performed directly on the papilla. The sample was stored in formol. Moreover, a first mapping of the chemical phase from the top of the papilla to the deep medulla is obtained. Direct structural evidence of the presence of ACCP as a major constituent is given for the first time. This set of data, coherent with previous studies, shows that this chemical phase can be considered as one precursor in the genesis of RP.

Keywords: X-ray absorption near-edge structure; pathological calcification; calcium phosphate; Randall's plaque; kidney stones.

1. Introduction

The significant increase in the prevalence of attached kidney stones in calcium oxalate stone formers (48 to 100%) has attracted a great deal of attention (Daudon *et al.*, 2010; Matlaga *et al.*, 2006). This structural particularity may explain the dramatic increase in urolithiasis now affecting up to 20% of the population in the industrialized countries. It is noteworthy that, among the explanation of such epidemic increases, an intimate correlation between urolithiasis and other major public health problems such as type-2 diabetes mellitus has been underlined.

At the surface of attached kidney stones, a particular deposit termed Randall's plaque (RP) serves as a nucleus (Evan *et al.*, 2006; Matlaga *et al.*, 2007). Since the pioneering work of Randall (1936, 1937, 1940), different models have been discussed to explain the formation of RP. We have to recall that most umbilicated stones formed on a renal papilla contain whewellite (calcium oxalate monohydrate) as the main component and we have already discussed the mechanism of formation of such stones on apatite RP (Daudon *et al.*, 2007). Regarding the pathogenesis of RP, if convincing arguments have shown that the plaque is initiated in the inner medulla and progressively expands to the papillary epithelium (Evan *et al.*, 2003), other experimental facts based on the evaluation of the carbonate groups by Fourier transform infrared spectroscopy (FT-IR) seem to show that other mechanisms have to be considered. Recently, Vervaet *et al.* (2009) have underlined the fact that interstitial nephrocalcinosis in the context of RP formation does not seem to be associated with any kind of prior tubulo-interstitial morphological aberration.

Regarding the chemical composition, even if other phosphate phases such as whitlockite or brushite can be found as

minor components (less than 5%), calcium phosphate apatite (CA) as well as amorphous carbonated calcium phosphate (ACCP) are the major components of most RPs. As underlined previously for biological apatites (Bazin *et al.*, 2009*a*,*b*), their nanometer size with an anisotropy along the *c* axis (Vallet-Regı & Gonzalez-Calbet, 2004) is combined with a high Ca and OH deficiency (Wilson & Elliott, 1999; Rey *et al.*, 1995). At their surface, carbonate groups (Penel *et al.*, 1998) as well as an amorphous part (ACCP) (Rey *et al.*, 2007*a*; Cazalbou *et al.*, 2004) can be found. Of note, ACCP can be considered as a precursor for CA. Even if several studies have been dedicated to the study of RP, only a few structural investigations have been performed *ex vivo*.

In order to provide structural data on urolithiasis, numerous techniques have been used including micro-CT (Miller *et al.*, 2008), scanning electron microscopy (Daudon *et al.*, 2008, 2009), thermal analysis (Gosh *et al.*, 2009), FT-IR spectroscopy (Quy Dao & Daudon, 1997), atomic force microscopy (Rez *et al.*, 2002), as well as techniques specific to large instruments (Bazin *et al.*, 2006) such as proton-induced X-ray emission (Pineda-Vargas *et al.*, 2009), powder neutron diffraction (Daudon *et al.*, 2009), synchrotron radiation micro-X-ray fluorescence (Bazin *et al.*, 2007) or micro-X-ray diffraction (Fleming *et al.*, 2003; Ancharov *et al.*, 2007). Very early XAS studies have been undertaken on apatites (Harries *et al.*, 1986; Hesterberg *et al.*, 1999) and, more recently, kidney stones have been investigated through X-ray absorption spectroscopy (Bazin *et al.*, 2008).

X-ray absorption spectroscopy (XAS) is especially useful for characterizing biological calcium phosphates for several reasons. First, calcified deposits and their model compounds may be poorly crystalline or amorphous and consequently difficult to characterize by X-ray powder diffraction. Second, the size of the probe is sufficient to establish a mapping of a biological sample for which no specific preparation is necessary. XAS includes X-ray absorption near-edge structure (XANES) and extended X-ray absorption fine structure (EXAFS) and is able to describe accurately the electronic state, the geometry of the very first neighbors and finally the first coordination spheres of a selected element. The present study is based on the XANES part of the X-ray absorption spectra to evaluate the local environment of Ca atoms (Harries *et al.*, 1986). The spectra of possible Ca species, namely ACCP and CA compounds, in the papilla were measured. Moreover, owing to the submillimeter size of the probe, we will establish a mapping of these compounds from the top of the papilla where the RP is localized to the medulla.

2. Materials and methods

2.1. Experimental design

The biological samples used in the present investigation came from two different hospitals. More precisely, kidney stones, which were used as reference compounds for biological calcium phosphates (CA, ACCP), came from Necker Hospital while the two studied papillae came from two different kidneys at Nice Hospital after nephrectomy for tumor (Fig. 1). The kidney was obtained after a radical enlarged nephrectomy for a single tumor (clear cell carcinoma) on the cortex far away from the upper urinary tract. The presence of RPs was confirmed by direct examination opening the anatomopathological piece under a stereomicroscope. A large fragment of the kidney opposite the tumor was dissected, conserving the entire Malpighi's pyramid. The samples were stored in formol and then positioned directly under the beam. This protocol has been used in order to preserve the physicochemistry integrity of the sample. The synthetic hydroxyapatite (HAP) came from Biorad.

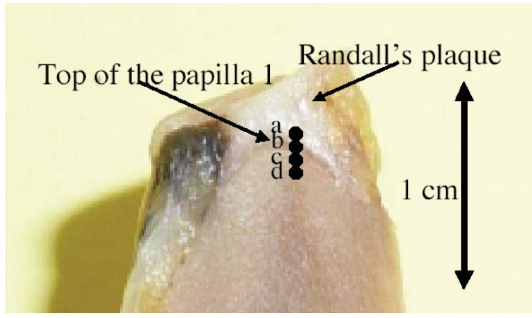

Figure 1
The RP can be clearly seen as the white part at the top of the renal papilla. *a*, *b*, *c* and *d* refer to acquisition points related to X-ray absorption experiments.

2.2. Fourier transform infrared spectroscopy

Samples used for reference compounds (HAP, CA and ACCP) were first characterized by FT-IR using a spectrometer (Vector 22; Bruker Spectrospin, Wissembourg, France) according to an analytical procedure previously defined (Estepa & Daudon, 1997). Data were collected in the absorption mode between 4000 and 400 cm^{-1} with a resolution of 4 cm^{-1}. The different absorption bands of the calcium phosphate apatite are well assigned (Fig. 2). The ν_1 and ν_3 P—O stretching vibration modes are measured at 960–962 cm^{-1} and 1035–1045 cm^{-1}, respectively, while the ν_4 O—P—O bending mode corresponds to the doublet at 602–563 cm^{-1}. The bands at 3570 and 633 cm^{-1} corresponding to the stretching and vibrational modes of the OH^- groups are present for the HAP and almost absent for the biological apatites (CA and ACCP). A key point in the analysis is linked to the presence of a shoulder in the ν_3 absorption band which can be used as a fingerprint for the presence of the ACCP compound.

2.3. XAS at SOLEIL

The selected samples were investigated on the DIFFABS beamline (Fig. 3) situated at the D13-1 bending magnet at synchrotron SOLEIL (Saint Aubain, France). This beamline is mainly dedicated to structural characterization by combining, if necessary, X-ray diffraction, X-ray absorption and X-ray fluorescence spectroscopies (Baudelet *et al.*, 2005). In our case, the beamline was optimized in order to determine the elec-

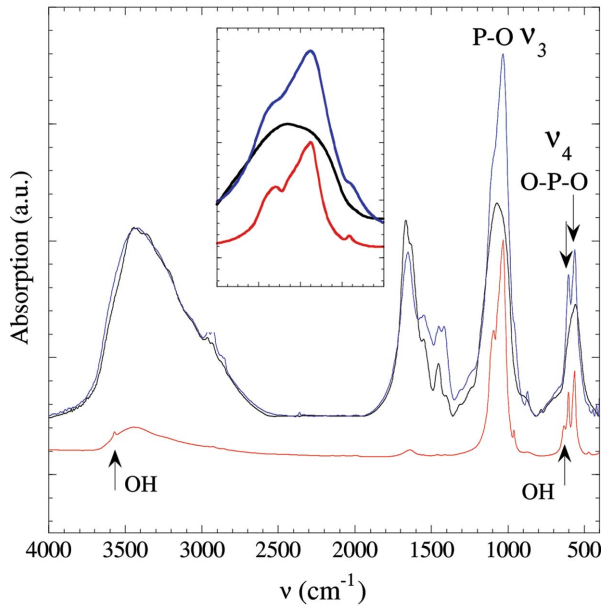

Figure 2
FT-IR absorption spectra for the compounds used here as references (in red, HAP; in blue, CA; in black, ACCP).

tronic state as well as to describe accurately the first coordination sphere of Ca atoms.

SOLEIL was running at 2.75 GeV with an average current of 300 mA for our experiments in the new TOP/UP configuration. To reach a monochromatic and focused X-ray beam at the sample position, a 'standard' main optic (for a bending-magnet source) was used. The monochromatization and horizontal focusing is achieved using a fixed-exit double Si(111) crystal monochromator. Upstream and downstream, two long cylindrical mirrors (50 nm Rh deposited on Si substrates) are used. The first one (between the source and the monochromator) allows the vertical beam to be collimated in order to increase the energy resolution. The second one focuses the monochromatic beam in the vertical direction. For these experiments, the angle of incidence of both mirrors was 6 mrad. Taking into account the Darwin width of the crystals

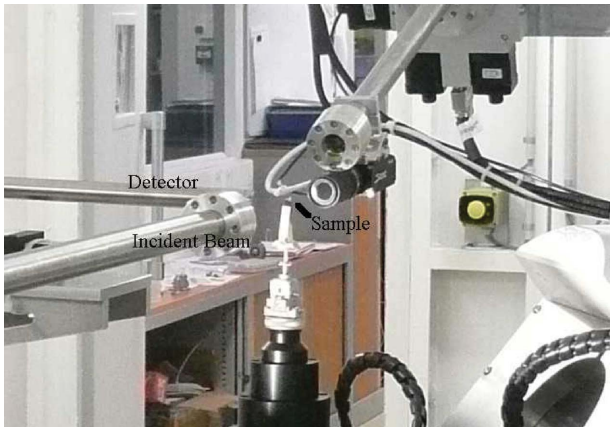

Figure 3
The DIFFABS experimental set-up showing the six-axis diffractometer and photography of the sample.

of the monochromator and the collimation of the first mirror, the optimized and repeatable energy resolution $\Delta E/E$ is 10^{-4} around the 4 keV range. At the sample position, the spot size was defined with slits to reach 100 µm × 250 µm (H × V, FWHM).

Regarding the Ca *K*-edge (4086 eV), the energy range was between 4020 and 4140 eV, with energy steps of 0.5 eV and 3 s dwell time per point. The size of the beam was determined by a set of slits (100 µm × 500 µm). To monitor the incident X-ray beam, a PIN Si photodiode coupled with Kapton foil as scatterer was used. XANES spectra were obtained in fluorescence mode from a silicon drift detector (SDD) (Röntec-Xflash; Sträuder *et al.*, 1998). The 5 mm^2 SDD was placed at 90° to the incident beam, in the horizontal plane in order to minimize the elastic beam scatter contribution. The distance between the sample and the SDD can be modified, depending on the fluorescence emission. Energy calibration was achieved using a well crystallized synthetic HAP.

For the X-ray fluorescence experiments, different compounds used as reference (HAP, CA and ACCP) were previously ground to a smooth powder in an agate mortar and sieved to obtain regularity in size. In order to obtain X-ray fluorescence measurements, the different reference compounds were then diluted in a polymer. Note that regarding the two papillae, the water content was preserved during the acquisition procedure.

3. Results and discussion

At either the *K*- or the *L*-edge, XANES contains both electronic and structural information, but can be difficult to interpret fully (Bazin & Rehr, 2003*a*; Veiga & Figueiredo, 2008; Fleet & Liu, 2009). It is commonly assumed that spectral features within ∼10 eV of the edge threshold are due to electronic transitions to unoccupied states near the Fermi level and are sensitive to the spatial and electronic details of the potential (Asokan *et al.*, 2001; Eichert *et al.*, 2005). In the case of nanometer-scale metallic clusters, such structures are sensitive to the size of the cluster (Bazin *et al.*, 1997; Bazin & Rehr, 2003*b*).

Regarding our experiments performed at the Ca *K*-edge (Fig. 4), the feature labeled A reflects the effective charge and the site symmetry of Ca^{2+} ions ($3d^0$ electron configuration). We consider now that transitions are discrete, with broadening owing to core-hole lifetime and instrumental resolution. Special attention has to be paid in the case of *L*-edges (Zaanen *et al.*, 1985; Fleet & Liu, 2009). Following this simple scheme, this feature A can be attributed to a $1s \rightarrow 3d$ transition or O 2*p* molecular orbital (Ravel & Stern, 1995). This transition is dipole forbidden ($\Delta l = 2$) and results from mixing of unoccupied *d* final states with *p*-character final states.

After this pre-peak A, we find the most intense resonance of the spectra, called the white line (Cauchois & Mott, 1949). This structure includes a shoulder-like structure (feature B; transition $1s \rightarrow 4s$) and a double peak (features C1 and C2; transition $1s \rightarrow 4p$) whose relative intensities depend on the type of Ca involved [Ca(I) or Ca(II)] (Eiden-Assmann &

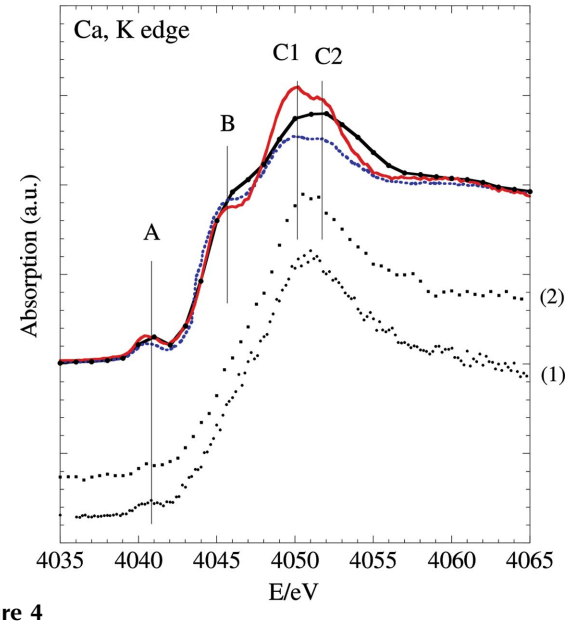

Figure 4
XANES spectra of different compounds: references (in red, HAP, well crystallized synthetic apatite; in blue, CA, biological apatite; in black, ACCP, amorphous biological apatites) and biopsies [(1) and (2) are the X-ray absorption spectra collected when the beam is positioned on the RP]. Details regarding the pre-peak A, the shoulder B and the double peaks C1–C2 are clearly visible.

Viertelhaus, 2000; Asokan *et al.*, 2001; Eichert *et al.*, 2005). At this point we would like to recall that HAP can be described as a hexagonal stacking of $(PO_4)^{3-}$ groups with two kinds of tunnel parallel to the *c* axis. The first one coincides with the ternary axis of the structure and is occupied by Ca^{2+}, noted as Ca(I) ions. The second one is linked by oxygen and other calcium ions, noted Ca(II), and is occupied by OH^- ions. Ca(I) and Ca(II) are present in a 2/3 ratio.

While the feature A is quite the same in the three samples HAP, CA and ACCP, significant variations are measured for the shoulder B as well as for the C1–C2 features (Fig. 4). These observations are in line with a previous investigation (Eiden-Assmann & Viertelhaus, 2000) where it was noted that this shoulder becomes more prominent as the crystallinity of the compounds increases. The XANES part is thus sensitive to the local order around Ca^{2+} cations, *i.e.* between the samples CA and ACCP. Note that this type of experimental approach has already been performed on apatitic and non-apatitic calcium phosphates of biological interest (Asokan *et al.*, 2001; Eichert *et al.*, 2005).

Owing to a significant increase in the prevalence of kidney stone formation on RP, the pathogenesis of RP has been the subject of several major studies mostly based on histology. Aside from structural investigations based purely on classical laboratory techniques, there were attempts to use synchrotron-related techniques to complete our knowledge of the biochemical process associated with the formation of RP. This literature includes *in vitro* studies where the conversion of amorphous calcium phosphate into hydroxyapatite has been investigated by EXAFS spectroscopy (Harries *et al.*, 1987) as well as the conversion between brushite and apatite (Lundager Madsen, 2008) and also *ex vivo* studies dedicated to the characterization of kidney stones (Orlando *et al.*, 2008) or the investigation of the influence of trace elements present in biological or synthetic apatites such as Zn (Takatsuka *et al.*, 2005; Tang *et al.*, 2009). Numerous results already published (Sowrey *et al.*, 2004) demonstrate that XANES is a very efficient tool for studying Ca compounds. The chemistry of Ca phosphate is quite complex. Among the different Ca phosphates present in kidney stones are brushite, octacalcium phosphate and whitlockite, each chemical phase being often linked to a specific pathology or risk factor. Regarding RP, an epidemiologic study based on 5401 umbilicated calculi, of which 91.5% had an identifiable plaque, has shown that CA and ACCP are the major components (Daudon *et al.*, 2007). It was logical to extend this type of XANES work to investigate the localization of pathological calcification inside papilla.

In Fig. 4 is plotted the first XANES part of the absorption spectra, collected at the top of the papilla for the two samples. Obviously, the pre-peak A linked to the 2+ electronic state of Ca atoms is present. More interestingly, the fact that the shoulder B is absent along with a single feature instead of C1 and C2 structures demonstrate that the Ca phosphate compound is closer to ACCP than the more crystalline standards. Because only the major component gives a significant part of the X-ray absorption spectra, it is possible that other Ca phosphates are present as minor phases as well. This first experimental observation is in line with *in vitro* studies which have underlined the formation of such a compound before the formation of Ca phosphate apatites. As pointed out by Rey *et al.* (2007*b*), it seems to exist in its nascent state only in wet samples and is altered on drying. This chemical property has biological implication linked to exchange properties with foreign cations (Cazalbou *et al.*, 2005) as well as the interactions between apatite and tissues. Here, it is quite clear that the fixation of apatite on the epithelium is dependent on this hydrated layer. It is possible that the drying process occurring before FT-IR experiments may alter the physicochemical integrity of the sample and that part of the CA comes from a chemical transition from ACCP.

In Fig. 5 we show the different X-ay absorption spectra collected when we move from the top of the renal papilla to the medulla (Fig. 1). The amplitude (1a for the spectra a) of the absorption edge (from 1a to 1d in Fig. 5) and thus the Ca content decreases rapidly. This is mainly due to the presence of the calcification at the top of the papilla. The feature A, which corresponds to the fact that the electronic state of calcium is 2+, is clearly visible. The position of the features B, C1 and C2 which are very sensitive to the crystallinity of the calcification at the edge have been indicated. Of interest, note that the morphology of feature B in papilla 1 is close to the morphology of feature B in ACCP (Fig. 4). Moreover, the two features C1–C2 are not present at the top of the absorption spectra. These two observations give direct structural evidence that one of the biochemical mechanisms can be described as an agglomeration of ACCP entities in the medulla leading to the formation of RP at the top of the papilla. Regarding the papilla 2 (Fig. 6), similar observations can be made regarding

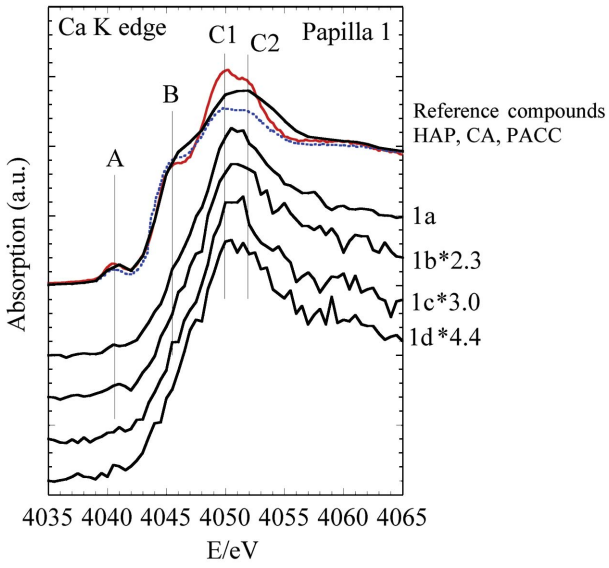

Figure 5
XANES part of the absorption spectra for the papilla 1.

feature B, which is clearly close to that corresponding to the ACCP compound.

This set of *ex vivo* experimental results are in line with the data reported for two papilla samples recently published (Evan *et al.*, 2007). In this paper the authors found that carbapatite layers alternating with proteins may form the upper part of the plaque at the surface of the papilla. By FT-IR microscopy, they observed that carbapatite might be mixed with a poorly crystalline phase while, within the tissue, carbapatite appeared well crystallized. In contrast, our data suggest that the amorphous phase could be an important part of the calcium phosphate deposited within the papilla. This apparent discrepancy can be linked to experimental conditions. Our *ex vivo* protocol helped us to preserve the physicochemical state of the sample, especially the state of crystallization which depends on the hydration level.

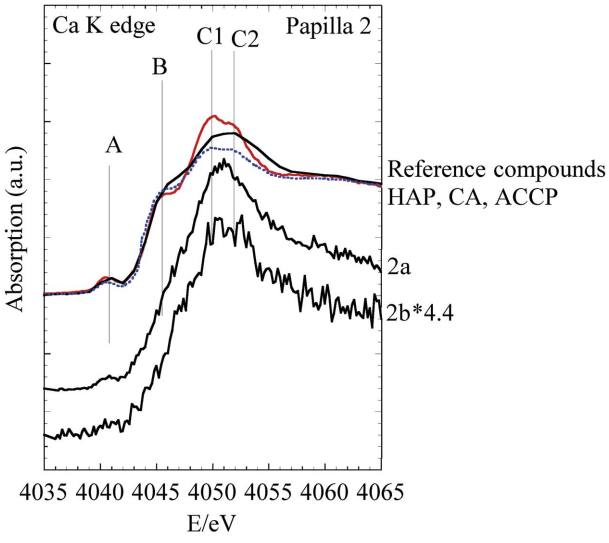

Figure 6
XANES part of the absorption spectra for the papilla 2.

4. Conclusion

We give for the first time direct structural evidence of the significant presence of an amorphous phase similar to ACCP as a major constituent of RP. This set of data shows that this chemical phase can be considered as one precursor in the genesis of RP. Moreover, our measurements suggest that ACCP may be deposited within the tissue, and not only at the surface of the papilla.

This work was supported by the Physics and Chemistry Institutes of CNRS and by contract ANR-09-BLAN-0120-02.

References

Ancharov, A. I., Potapov, S. S., Moiseenko, T. N., Feofilov, I. V. & Nizovskii, A. I. (2007). *Nucl. Instrum. Methods Phys. Res. A*, **575**, 221–224.
Asokan, K., Jan, J. C., Chiou, J. W., Pong, W. F., Tseng, P. K. & Lin, I. N. (2001). *J. Synchrotron Rad.* **8**, 839–841.
Baudelet, F. *et al.* (2005). *Rev. Inst. Fr. Petrol.* **60**, 849–874.
Bazin, D., Carpentier, X., Brocheriou, I., Dorfmuller, P., Aubert, S., Chappard, Ch., Thiaudière, D., Reguer, S., Waychunas, G., Jungers, P. & Daudon, M. (2009*a*). *Biochimie*, **91**, 1294–1300.
Bazin, D., Carpentier, X., Traxer, O., Thiaudière, D., Somogyi, A., Reguer, S., Waychunas, G., Jungers, P. & Daudon, M. (2008). *J. Synchrotron Rad.* **15**, 506–509.
Bazin, D., Chappard, Ch., Combes, Ch., Carpentier, X., Rouzière, S., André, G., Matzen, G., Allix, M., Thiaudière, D., Reguer, S., Jungers, P. & Daudon, M. (2009*b*). *Osteopor. Int.* **20**, 1065–1075.
Bazin, D., Chevallier, P., Matzen, G., Jungers, P. & Daudon, M. (2007). *Urol. Res.* **35**, 179–184.
Bazin, D., Daudon, M., Chevallier, P., Rouzière, S., Elkaim, E., Thiaudière, D., Fayard, B., Foy, E., Albouy, P. A., André, G., Matzen, G. & Veron, E. (2006). *Ann. Biol. Clin.* **64**, 125–139.
Bazin, D. & Rehr, J. (2003*a*). *Catal. Lett.* **87**, 85–90.
Bazin, D. & Rehr, J. (2003*b*). *J. Phys. Chem. B*, **107**, 12398–12402.
Bazin, D., Sayers, D. & Rehr, J. (1997). *J. Phys. Chem.* **101**, 11040–11050.
Cauchois, Y. & Mott, N. F. (1949). *Philos. Mag.* **40**, 126–130.
Cazalbou, S., Eichert, D., Drouet, Ch., Combes, Ch. & Rey, Ch. (2004). *C. R. Palevol.* **3**, 563–572.
Cazalbou, S., Eichert, D., Ranz, X., Drouet, C., Combes, Ch., Harmand, M. F. & Rey, Ch. (2005). *J. Mater. Sci. Mater. Med.* **16**, 405–409.
Daudon, M., Bazin, D., Jungers, P., André, G., Cousson, A., Chevallier, P., Véron, E. & Matzen, G. (2009). *J. App. Cryst.* **42**, 109–115.
Daudon, M., Jungers, P. & Bazin, D. (2008). *N. Engl. J. Med.* **359**, 100–102.
Daudon, M., Traxer, O., Jungers, P. & Bazin, D. (2007). *AIP Conf. Proc.* **900**, 26–34.
Daudon, M., Traxer, O., Williams, J. C. Jr & Bazin, D. (2010). In *Urinary Tract Stone Disease*, edited by N. Rao, J. Khavanagh and G. Preminger. Berlin: Springer. In the press.
Eichert, D., Salomé, M., Banu, M., Susini, J. & Rey, Ch. (2005). *Spectrochim. Acta B*, **60**, 850–858.
Eiden-Assmann, S. & Viertelhaus, M. (2000). *HASYLAB Jahresber. 1999.* HASYLAB/DESY, Hamburg, Germany.
Estepa, L. & Daudon, M. (1997). *Biospectroscopy*, **3**, 347–355.
Evan, A. P., Coe, F. L., Lingeman, J. E., Hao, Y., Sommer, A. J., Bledsoe, S. B., Anderson, J. C. & Worcester, E. M. (2007). *Anat. Rec.* **290**, 315–323.
Evan, A. P., Lingeman, J., Coe, F. L. & Worcester, E. (2006). *Kidney Int.* **69**, 1313–1318.

Evan, A. P., Lingeman, J. E., Coe, F. L., Parks, J. H., Bledsoe, S. B., Shao, Y., Sommer, A. J., Paterson, R. F., Kuo, R. L. & Grynpas, M. (2003). *J. Clin. Invest.* **111**, 607–616.
Fleet, M. E. & Liu, X. (2009). *Am. Mineral.* **94**, 1235–1241.
Fleming, D. E., Van Riessen, A., Chauvet, M. C., Grover, P. K., Hunter, B., Van Bronswijk, W. & Ryall, R. L. (2003). *J. Bone Miner. Res.* **18**, 1282–1291.
Gosh, S., Basu, S., Chakraborty, S. & Mukherjee, A. K. (2009). *J. App. Cryst.* **42**, 1–7.
Harries, J. E., Hukins, D. W. L. & Hasnain, S. S. (1986). *J. Phys. Colloq.* **47**, C8-603–C8-606.
Harries, J. E., Hukins, D. W. L., Holt, C. & Hasnain, S. S. (1987). *J. Cryst. Growth*, **84**, 563–570.
Hesterberg, D., Zhou, W., Hutchison, K. J., Beauchemin, S. & Sayers, D. E. (1999). *J. Synchrotron Rad.* **6**, 636–638.
Lundager Madsen, H. E. (2008). *J. Cryst. Growth*, **310**, 2602–2612.
Matlaga, B. R., Coe, F. L., Evan, A. P. & Lingeman, J. E. (2007). *J. Urol.* **177**, 31–38.
Matlaga, B. R., Williams, J. C. Jr, Kim, S. C., Kuo, R. L., Evan, A. P., Bledsoe, S. B., Coe, F. L., Worcester, E. M., Munch, L. C. & Lingeman, J. E. (2006). *J. Urol.* **175**, 1720–1724.
Miller, N. L., Williams, J. C., Humphreys, M. R., Bledsoe, S. B., Handa, S. E., Jackson, M. E., Evan, A. P. & Lingeman, J. E. (2008). *J. Urol.* **179**, 587–588.
Orlando, M. D. T., Kuplich, L., de Souza, D. O., Belich, H., Depianti, J. B., Orlando, C. G. P., Medeiros, E. F., da Cruz, P. C. M., Martinez, L. G., Corrêa, H. P. S. & Ortiz, R. (2008). *Powder Diffr. Suppl.* **23**, S59–S64.
Penel, G., Leroy, G., Rey, Ch. & Bres, E. (1998). *Calcif. Tissue Int.* **63**, 475–481.
Pineda-Vargas, C. A., Eisa, M. E. M. & Rodgers, A. L. (2009). *Appl. Radiat. Isot.* **67**, 464–469.
Quy Dao, N. & Daudon, M. (1997). *Infrared and Raman Spectra of Calculi.* Paris: Elsevier.
Randall, A. (1936). *N. Engl. J. Med.* **214**, 234–237.
Randall, A. (1937). *Ann. Surg.* **105**, 1009–1027.
Randall, A. (1940). *J. Urol.* **44**, 580–589.
Ravel, B. & Stern, E. A. (1995). *Physica B*, **208**–**209**, 316–318.
Rey, Ch., Combes, Ch., Drouet, C., Lebugle, A., Sfihi, H. & Barroug, A. (2007*b*). *Materialwiss. Werkst.Tech.* **38**, 996–1002.
Rey, Ch., Combes, Ch., Drouet, C., Sfihi, H. & Barroug, A. (2007*a*). *Mater. Sci. Eng.* **27**, 198–205.
Rey, Ch., Miquel, J. L., Facchini, L., Legrand, A. P. & Glimcher, M. J. (1995). *Bone*, **16**, 583–586.
Rez, P., Fongand, H. & Sarikaya, M. (2002). *Microsc. Microanal.* **8**, 746–747.
Sowrey, F. E., Skipper, L. J., Pickup, D. M., Drake, K. O., Lin, Z., Smith, M. E. & Newport, R. J. (2004). *Phys. Chem. Chem. Phys.* **6**, 188–192.
Sträuder, L., Meidinger, N., Stäotter, D., Kemmer, J., Lechner, P., Leutenegger, P., Soltau, H., Eggert, F., Rohde, M. & Schäulein, T. (1998). *Microsc. Microanal.* **4**, 622–631.
Takatsuka, T., Hirano, J., Matsumoto, H. & Honma, T. (2005). *Eur. J. Oral Sci.* **113**, 180–183.
Tang, Y., Chappell, H. F., Dove, M. T., Reeder, R. J. & Lee, Y. J. (2009). *Biomaterials*, **30**, 2864–2872.
Vallet-Regı, M. & Gonzalez-Calbet, J. M. (2004). *Prog. Solid State Chem.* **32**, 1–31.
Veiga, J. P. & Figueiredo, M. O. (2008). *Appl. Phys. A*, **92**, 229–233.
Vervaet, B. A., Verhulst, A., D'Haese, P. C. & De Broe, M. E. (2009). *Nephrol. Dial. Transplant.* **24**, 2030–2035.
Wilson, R. M. & Elliott, J. C. (1999). *Am. Mineral.* **84**, 1406–1414.
Zaanen, J., Sawatsky, G. A., Fink, J., Speirer, W. & Fuggle, J. C. (1985). *Phys. Rev. B*, **32**, 4905–4913.